Journal of Innovative Optical Health Sciences
Vol. 7, No. 2 (2014) 1350041 (14 pages)

DOI: 10.1142/S1793545813500417

World Scientific
www.worldscientific.com

Intracellular oxygen: Similar results from two methods of measurement using phosphorescent nanoparticles

David Lloyd[*,§], Catrin F. Williams[*], K. Vijayalakshmi[†], M. Kombrabail[†], Nick White[*], Anthony J. Hayes[*], Miguel A. Aon[‡] and G. Krishnamoorthy[†]

[*]*Biosciences and School of Optometry and Vision Sciences*
Cardiff University, Cathays Park and Maindy Road, Cardiff, Wales, UK

[†]*Department of Chemical Sciences, Tata Institute of Fundamental Research*
Homi Bhabha Road, Mumbai 400 005, India

[‡]*The Johns Hopkins University, Institute of Molecular Cardiobiology,720 Rutland Av., 1059 Ross Bldg., Baltimore MD, USA*
[§]*lloydd@cf.ac.uk*

Received 30 June 2013
Accepted 1 September 2013
Published 8 October 2013

The ability to resolve the spatio-temporal complexity of intracellular O_2 distribution is the "Holy Grail" of cellular physiology. In an effort to obtain a minimally invasive approach to the mapping of intracellular O_2 tensions, two methods of phosphorescent lifetime imaging microscopy were compared in the current study and gave similar results. These were two-photon confocal laser scanning microscopy with pinhole shifting, and picosecond time-resolved epi-phosphorescence microscopy using a single 0.5 μm focused spot. Both methods utilized Ru coordination complex embedded nanoparticles (45 nm diameter) as the phosphorescent probe, excited using pulsed outputs of a titanium–sapphire Tsunami lasers (710–1050 nm).

Keywords: Time-resolved phosphorescence; intracellular O_2; two-photon excitation; pinhole shifting.

1. Introduction

Despite 50 years of research, uncertainties and controversies revolve around published values for tissue and intracellular pO_2. Many diverse methods have been employed; all are subject to problematic aspects and minimally non-invasive approaches are continually being devised. The complexity of the processes of human energy generation and

homeodynamics is nowhere more evident than in the O_2-delivery system to tissues, cells, and reaction sites.[1] This process displays a series of step-wise decreasing O_2 levels from alveolar air in equilibrium with arterial blood (containing the equivalent of 100 μM O_2) to the discharge of blood oxyhaemoglobin (depending on CO_2 tension) occurring with the range 80–20 mm Hg = 60–30 μM O_2. The oxymyoglobin store of red muscle begins to unload at below 10 μM O_2 and the working pO_2 in active skeletal muscle is only about 3 mm Hg.[2] The mean O_2 levels of some other human tissues are also unexpectedly low, e.g., 6–16 mm Hg in white brain cortex,[3] and 8 mm Hg in kidney medulla.[4] In the perifovea, the $P(O_2)$ was 48 ± 13 mm Hg (mean and SD) at the choroid and fell to a minimum of 3.8 ± 1.9 mm Hg around the photoreceptor inner segments in dark adaptation, rising again toward the inner retina, and 5 mm Hg at the retina.[5] Even in the rat gut, values of 58, 32, 11, and 3 mm Hg were determined in stomach, duodenum, small intestine-colon junction, and hind-colon.[6] The measurement of intracellular O_2 for cells *in vitro* should not only be appropriate to these values for their *in vivo* niches but also take into account the further complexities of heterogeneous dissolved gas distributions inside cells.

Oxygen and its reduced products are essential not only for energy production,[7] but also for the maintenance of appropriate redox balance[8] and cell signalling.[9] Reasons for wishing to resolve and map O_2 inside cells fall into several categories. The high respiratory activity of mitochondria is responsible for $> 90\%$ of O_2 consumption of the human organism, and oxidative phosphorylation is the major mitochondrial role. The high affinity of cytochrome *c* oxidase, the binuclear Cu–Fe haemoprotein, reacts by way of a multi-stage cyclic mechanism whereby a concerted and highly efficient four electron reduction of O_2 on the inner surface of the inner mitochondrial membrane (Km $O_2 <$ 0.1 μM),[10] leads to a residual steady-state level of O_2 that has not yet been accurately assessed. This can, however, be estimated indirectly by *in situ* non-invasive observations of the redox states of respiratory chain components using fluorimetric monitoring for NAD(P)H,[11] and spectrophotometric measurements for flavoproteins and cytochromes.[12,13] Thus respiratory chain mediated electron transport leads to depletion in the matrix space and the zones outside their outer membranes in their cytosolic vicinities. It has often been assumed that the sensing of O_2 is one of the many functions of mitochondria. However the discovery of a less sensitive but more suitably poised system, the HIF signalling pathway[14] that reacts during impending hypoxic conditions, and cooperates with mitochondrial O_2 sensing[15] emphasises the roles of several distinct proline hydroxylases with poorer oxygen affinities. Thus complexity of multicomponent fuctional reactivities can ensure a graded scale of responses.

The well established signalling functions of the single electron reduction products of O_2 utilization (especially $O_2-.$, and H_2O_2) provides another reason for determining local O_2 concentrations, as redox states and reaction rates both hinge on these values. During pathophysiological deprivation or transient interruption of oxygenation, the O_2 demand of tissue function cannot be satisfied so that adaptation to hypoxia necessitates forewarning. Thus a range of mechanisms each responsible for sensing different levels of low O_2 covers a wide ranging necessity for survival of viable cells and tissues: clearly the regulation is tuned for the particular needs of individual sites within the organism. In many microorganisms, and especially in bacteria inhabiting low-oxygen environments, affinities for O_2 are very high.[16] Thus, in *Escherichia coli*, the cytochrome *bd* has a Km O_2 of 5 nM O_2[17] during infections that involve invasion by intracellular bacteria, or in heavily infected tissues intracellular O_2 may reach extremely low levels.

The "Holy Grail" of cellular physiology is to resolve the spatio-temporal complexity of intracellular O_2 distribution by constructing 4D maps. Although two-photon excitation enables their dynamic imaging[18] quantification of the various species of reactive O_2 (OH., $O_2-.$, H_2O_2 and singlet O_2) in the past has largely relied on indirect data and has been often overestimated.[19] On the macroscopic scale, the dynamic distribution of O_2 *in vivo* in body fluids, tissues and organs continues to be an important research aim, and a number of fluorophores and luminophores have been used for this purpose[1,20,21]: many of the most important features of delivery of O_2 to tissues have emerged. Fluorescence lifetimes of organic fluorophores are mostly of the order of 10–20 ns and the diffusion path of a small molecule is very short.[22] Extra time during which diffusion may occur greatly increases the volume of solution that influences the excited

state of each fluorophore molecule.[23] Thus for some exceptionally long-lived cases, e.g., pyrenebutyric acid (100 ns in air-saturated water), the O_2-sensing sphere of influence of the probe is increased from 100 to 1000 times over that volume affecting the shorter lived excited molecules. Exceptionally long-lived fluorescent states such as this have been employed for O_2-mapping in living cells, e.g., in cultured cells of mouse liver by the use of quantitative fluorescence microscopy,[24] and in *Amoeba proteus*.[25] The even longer lifetimes provided by O_2-quenchable phosphorescent luminophores,[26–29] together with their other desirable photophysical properties,[30–35] make them substances of choice for a burgeoning body of applications.

For O_2 sensing, Ru(II) complexes show many advantages.[27,36,37] Lifetime measurements[38–40] obviate or minimize some of the deficiencies of intensity determinations especially with respect to environmental influences (local concentration of fluorophore and variation in excitation intensity, collection efficiency, propinquity to hydrophobic proteins or membranes, gradients of pH or ionic strength, etc.[41,42] Encapsulation in porous nanoparticles goes a further stage to making reliable intracellular assessments.[43–47]

In this paper, we show that two independent approaches, namely pinhole shifting in a two-photon excitation beam and epi-phosphorescence time-correlated single photon counting (TCSPC), give similar estimates of local O_2 concentrations within several different single-celled organisms and in suspensions of cultured mammalian cells. Some of these data have been published in preliminary form in a "Technical Design Note" note.[48]

2. Materials and Methods

2.1. *Yeast and Spironucleus cultures*

The yeasts *Schizosaccharomyces pombe* 972 h- and *Saccharomyces cerevisiae* were maintained and grown on Petri dishes containing Sabouraud Maltose Agar (Difco). Organisms were transferred to unbaffled Ehrlenmayer flasks (50 mL) containing 10 mL YEPD liquid medium (0.3% yeast extract, 1% peptone, and 1% glucose) and grown at 30°C for two days on a rotary shaker at 150 rpm. Before electroporation, repeated centrifugation for 3 min at 2000 rpm (3000 g min) and re-suspension in 1.0 M sorbitol solution removed all nutrients. Spironucleus vortens was cultured as described by Millet *et al.*[49]

2.2. *Human cells*

Cultured cell lines, human mammary adenocarcinoma, MCF-7, were from the European Collection of Cell Cultures, Porton Down, Wiltshire, UK. Human fibroblasts (human dermal fibroblast (HDF) cells) were from TIFR Biology stocks. Cancer cells and HDF were maintained in Eagles Minimal Essential Medium supplemented with 10% foetal bovine serum, penicillin and streptomycin. Detachment from the plastic culture flasks was carried out using trypsin/EDTA and was followed by re-suspension in growth medium.

2.3. *Nanoparticle preparation*

The Ru coordinate complex employed as a phosphorescent probe here has been extensively used and has proven a highly efficient O_2 sensor. Reagents (from Sigma-Aldrich) were $RuCl_3$ (57 mg, 0.0276 mmol) and 4,7-diphenyl-1, 10-phenanthroline disulfonic acid disodium salt (518 mg, 0.0965 mmol) in 20 mL distilled water refluxed with stirring for two days. After filtration and rotary evaporation, the product, $Ru([dpp(SO_3Na)_2]_3)Cl_2 \cdot 6H_2O$, was passed down a Sephadex G25 size exclusion column and eluted with water. The first brown and purple fractions were discarded and the red fraction dried. The product is $Ru([dpp(SO_3Na)_2]_3)Cl_2 \cdot 6H_2O$ and it contains several isomers with the $-SO_3Na$ substituents randomly positioned on the phenyl rings. However, previous reports indicate that the mixture of isomers gives no evidence of heterogeneous fluorescent lifetimes. Characterization of the compound by standard methods was performed as described.[37] The nanosensors were prepared by incorporation of $Ru([dpp(SO_3Na)_2]_3Cl_2 \cdot 6H_2O$ by encapsulation using radical polymerization added drop-wise into a solution of 43 mL hexane, 3.08 g AOT and 1.59 g Brij30 in a round bottom flask. The monomer solution contained 2.7 g acrylamide, 0.8 g *N*,*N*-methylenebis(acrylamide), and 9 mL of 10 mM sodium phosphate buffer, pH 7.2, were added to the microemulsion. The solution was stirred under argon throughout the preparation and deoxygenated by three freeze–vacuum–thaw cycles using liquid nitrogen as freezing medium. To initiate the polymerization, 50 μL of a 10% (w/w) sodium bisulfite solution was added. The solution was kept under argon and stirred at room temperature for 2 h to ensure complete polymerization.

Hexane was removed by rotary evaporation and the remaining solution was re-suspended in 96% ethanol and transferred to an Amicon ultra-filtration cell model 8200 (Millipore Corp., Bedford, MA, USA). The solution was washed with 600 mL 96% ethanol in order to separate surfactants, unreacted monomers and excess proteins from the sensors using a 100 kDa filter under 2 bar pressure. The polymer particles containing Ru complex were then re-suspended in ethanol and passed through a suction filtration system (Millipore Corp., Bedford, MA) with a 0.025 μm nitrocellulose filter membrane and rinsed with 100 cm^3 ethanol. Hydrodynamic particle diameter (45 nm) was determined by right-angle light scatter of 632.8 nm laser light (HeNe) using a BI-200SM Goniometer (Brookhaven Inst., New York). Nanoparticles were stored at –18°C. Re-suspension (18 mg mL^{-1}) was in 1.0 M sorbitol and dispersion was by treatment with 20 kHz ultrasound for 30 s at 4°C at an amplitude providing the maximum cavitation intensity.

2.4. *Electroporation of nanoparticles into yeast, Sp. vortens, rat neonatal cardiomyocytes, or human cells*

The Biorad Labs Gene Pulser Transfection Apparatus (Bio-Rad Laboratories, CA) was fitted with a Capacitor Extender set at 450 V for yeasts and 340 V and 320 V for human cells or *S. vortens* (capacitance 900 μF, resistance 200 Ω). Electroporation vessels were of 400 μL working volume; three high voltage pulses were employed.

2.5. *Pinhole shifting with two-photon excitation confocal microscopy*

Ramshesh[50] and Ramshesh and Lemasters[51] have described time-resolved imaging of long-lifetime luminescence of Europium (Eu^{3+}) microspheres, and explored some aspects of the potential usefulness of the method for biological applications (e.g., O_2 sensing in feline myocytes). As in the original method used by these authors, we employed a Zeiss LSM510META NLO confocal microscope with a Coherent Chameleon 140 fs pulsed Ti–sapphire laser system (with integral pump lasers) for two-photon excitation at 900 nm. This excitation avoids much of the autofluorescence expected from shorter wavelengths and also the longer wavelengths reduce the level of detection of any un-blocked (reflected) IR since the PMTs are less sensitive. The single photon excitation peak is at 450 nm. While this is not definitely predictive of a two-photon peak at 900 nm (i.e., 2×) this was a natural wavelength to choose in the absence of other information. An analysis of excitation efficiency at all available wavelengths is quite difficult, given the many variables involved, and because of this we have yet to seek a better wavelength to use. We used about 20% of the maximum laser intensity at the specimen plane. The ruthenium nanoparticles were imaged through a 685 nm shortpass emission filter after beam separation by a 545 nm longpass dichroic mirror using a 40×1.3NA Plan-Neofluor (Zeiss) oil immersion. The 685 nm shortpass filter is an IR blocking filter specifically designed for multiphoton imaging, i.e., to block the reflection of the titanium–Saphire laser.

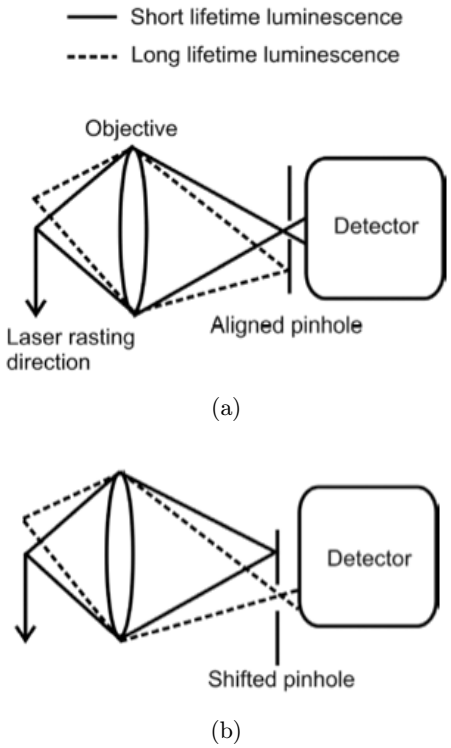

Fig. 1. The pinhole shifting technique. By shifting the pinhole successively out of its optimally aligned position (a), through a series of steps (e.g., b), collection of sequential time-delayed phosphorescence emission in the lagging direction of the raster scanned two-photon excitation is achieved by employing appropriate laser beam scanning speeds. Reproduced with permission from Ramshesh 2007.[50]

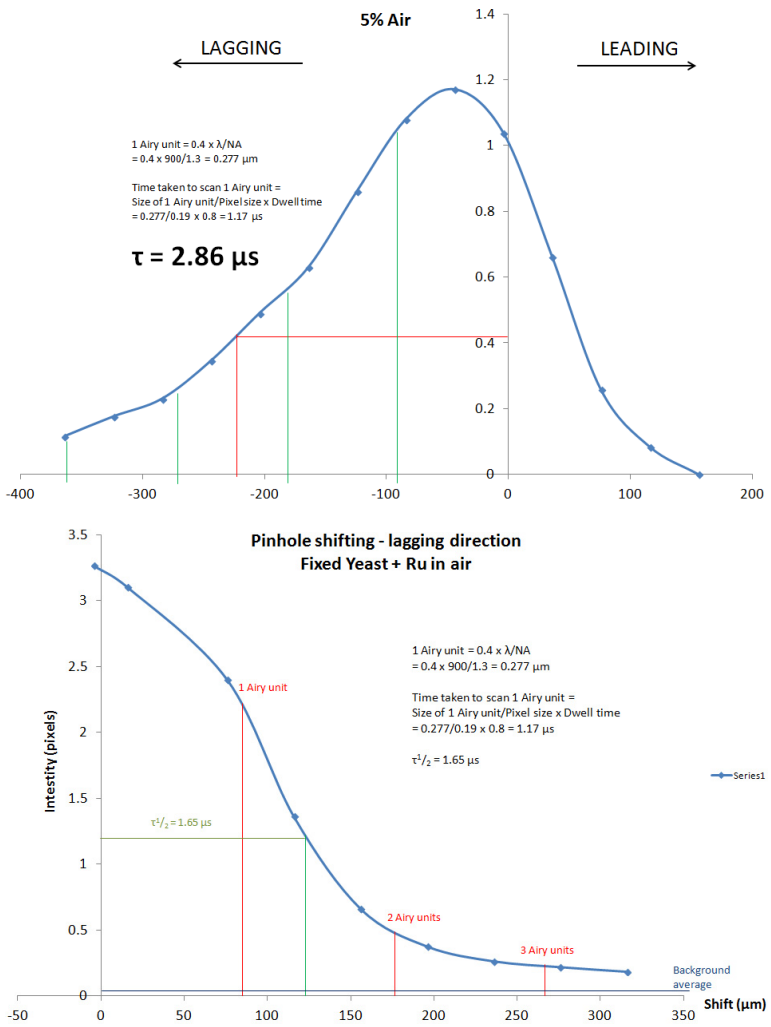

Fig. 2. Two examples of calculations of phosphorescence lifetime measurements from experiments with Ru nanoparticles in suspension or after electroporation into ethanol-fixed *Schizosaccharomyces pombe* that used the pinhole shifting method of Ramshesh and Lemasters.[51]

By collecting successive images from the shifted confocal of the raster scan, a series of images was collected. Image intensities were determined using the standard Zeiss LSM software and plotted as a function of decay times (Fig. 2) calculated from scan speed, pinhole offset and consequent image displacement from the optical axis).

2.6. *Epi-phosphorescence TCSPC*

The time-resolved fluorescence microscope was a combination of a picosecond time-resolved fluorescence spectrometer and an inverted epifluorescence microscope.[52] The time-resolved epi-phosphorescence measurements were carried out with a TCSPC setup coupled with a picosecond laser (Fig. 3).

A titanium–sapphire picosecond laser beam (Tsunami, Spectra Physics) pumped by a diode pumped CW Nd–vanadate laser (532 nm) (Millenia X, Spectra Physics), and frequency doubled by a doubler, was used to excite a single cell at 495 nm. The pulse width of the excitation laser beam was typically ~ 1 ps. A pulse repetition rate of 80 MHz was reduced to a repetition rate of 0.5 MHz by a pulse picker. The ps pulses obtained after frequency doubling were guided to the objective lens by a dichroic mirror and focused onto a single cell. The diameter of the focused beam was $\sim 0.5\,\mu$m and hence several locations within a single cell could be probed. Time-resolved epi-phosphorescence measurements were carried out on a Nikon Diaphot 300 microscope fitted with a 20× objective

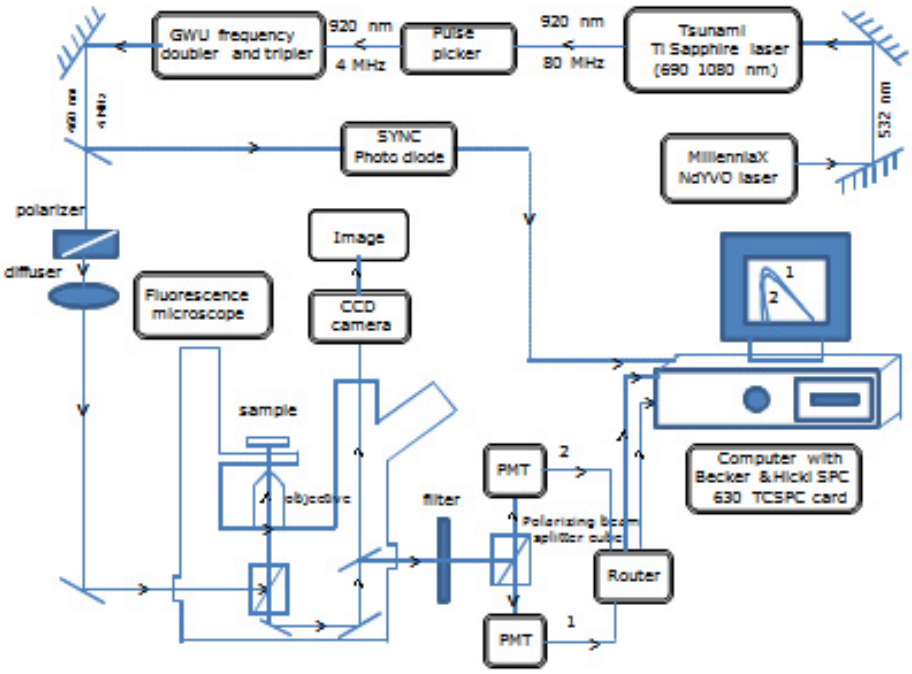

Fig. 3. Schematic diagram of the fluorescence microscope setup used for acquiring time-resolved epi-phosphorescence data on live cells. The main components are (i) a picosecond laser (ii) an inverted fluorescence microscope (iii) a TCSPC spectrometer.

with 0.75 NA maintained at room temperature (23°C). Phosphorescence emission collected by the same objective lens was passed through a combination of a cut-off filter (475 nm longpass and a shortpass filter (600 nm), and a polarizer. Time-resolution of the phosphorescence signal was obtained by coupling the microscope to a TCSPC card (Becker and Hickl, SPC-630). The temporal resolution of the setup is ~ 50 ps and the spatial resolution is $\sim 0.5\,\mu$m in the xy plane. The measurements typically require ~ 100 luminophore molecules in the observation volume. The instrument response function was estimated by the use of oxonol VI whose fluorescence lifetime is < 50 ps. The full width at half maximum height of the instrument response function estimated in this way was ~ 160 ps. Phosphorescence decays were analyzed for a single exponential function by using the nonlinear fitting. Since the repetition rate (0.5 MHz) of the excitation pulse was shorter than the measured lifetimes we ensured that our analysis took care of the incomplete decay coming from the previous excitation pulse. However, for single exponential decays this overlap does not cause any problem in the analysis even if the incomplete decays from previous pulses are not taken into account.

3. Results and Discussion

3.1. *Electroporation gives minimally-invasive permeabilization*

Figure 4 shows that electroporation is an effective method for loading cells and organisms with polyacrylamide nanoparticles containing the Ru coordinate complex. For all four populations of organisms, nanoparticles have entered all cells. Controls neither incubated nor electroporated with nanoparticles showed no autofluorescence at wavelengths in the red range of visible spectra (by confocal microscopy), or in the red channel in the two-photon scans. Some endosomal uptake of nanoparticles into MCF-7 cells occurred in the absence of electroporation.

The images indicate that, after electroporation in the presence of Ru nanoparticles using the mild conditions indicated, intracellular distributions are not confined to any specific subcellular organelles, although the distribution within a cell is heterogeneous and some organelles (e.g., nuclei) show lower intensity of emission. Absence of blebbing indicates vitality of the carcinoma cells. Similarly the continued motility of Spironucleus suggests the relatively innocuous nature of the permeablization procedure. Yeasts continued to

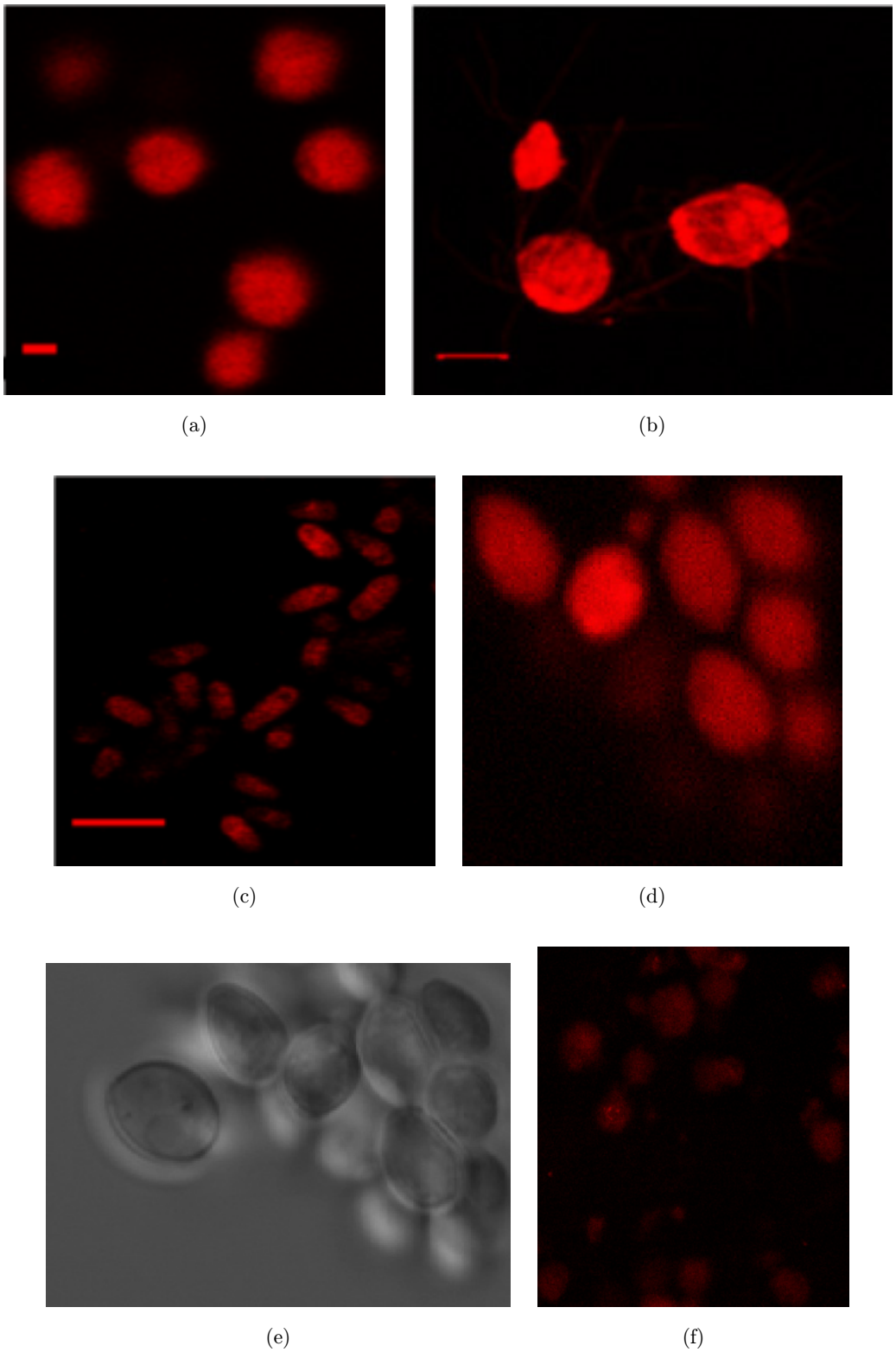

Fig. 4. Two-photon excitation scanning laser microscope images of Ru coordinate complex electroporated into: (a) human adenocarcinoma (MCF-7) cells, (b) the flagellated protist, *Spironucleus vortens*, (c) the fission yeast, *Schizosaccharomyces pombe*, (d) a confocal image of *Saccharomyces cerevisiae*, (f) rat neonatal cardiomyocytes using two-photon excitation. A Nomarski Differential Interference Contrast image of the yeast (e) is also shown. Untreated control cells and organisms (not exposed to or electroporated with nanoparticles) showed no red autofluorescence. Scale bars = 10 μm. Panels (a–c) reproduced from Williams *et al.*[48] with permission.

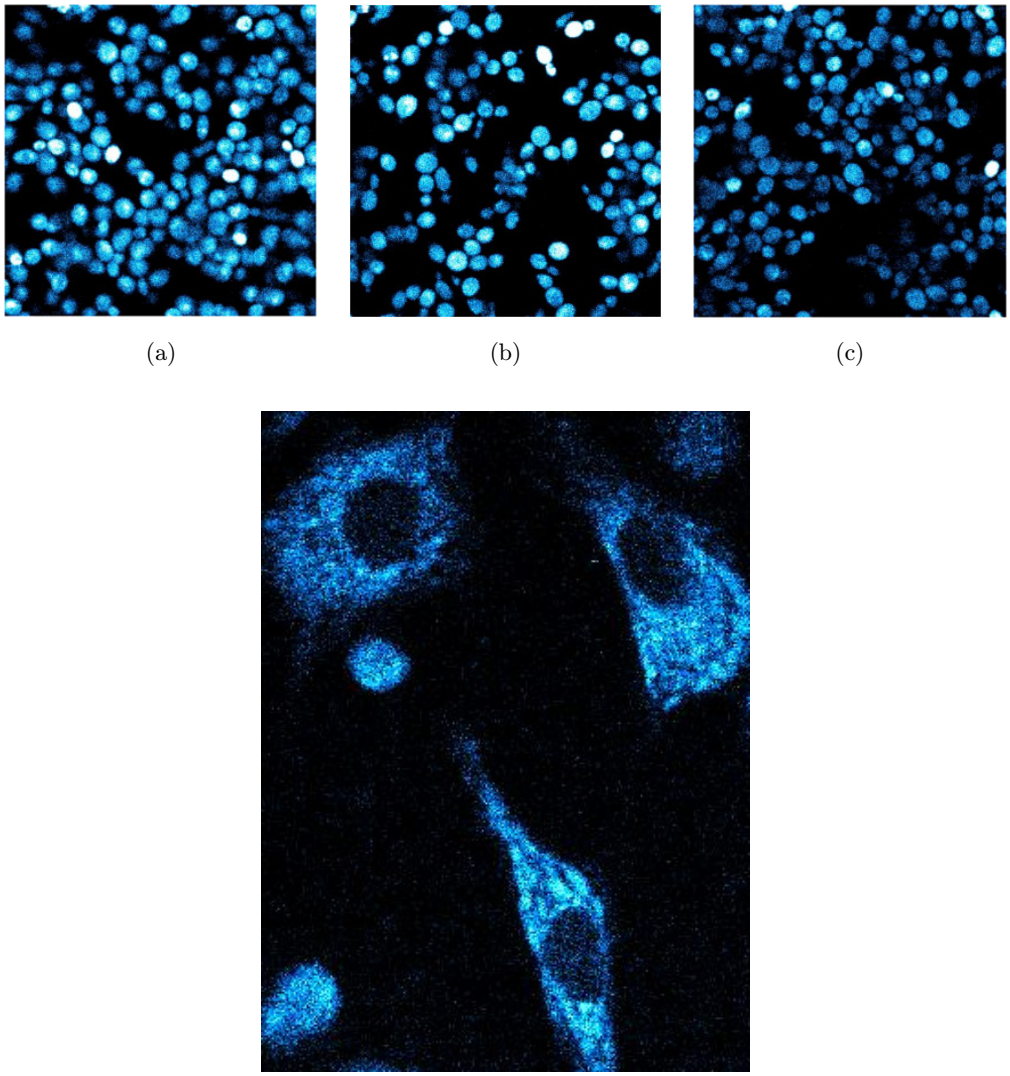

(a) (b) (c)

(d)

Fig. 5. Two-photon excitation of autofluorescence (excitation 740 nm, total emission < 490 nm), was almost entirely due to NAD(P)H: in *Saccharomyces cerevisiae* (a) before and (b) after, electroporation. In (c) and (d) yeast and cardiomyocyte fluorescence after electroporation in the presence of Ru nanoparticles confirm continued cellular redox balances. Mild ultrasonic treatment gave permeabilized control cells that showed negligible autofluorescence under these optical conditions.

proliferate so as to produce colonies on solid medium, and cardiomyocytes continued to spread and exhibit regular contractility.

For cardiomyocytes (Fig. 5), the persistence of NAD(P)H autofluorescence also confirmed continued cellular integrity.

3.2. *Response of the Ru nanoparticle probe to O_2*

Figure 6 shows images of the intensity of emission of nanoparticles in three MCF-7 cells during transitions from a N_2 gas phase to air and back. Both response times are limited by gaseous diffusion into the hanging drop cell suspension.

3.3. *Two-photon laser excitation scanning microscopy with pinhole shifting*

The optical setup whereby laser scanning microscopy may be to acquire sequential images with delayed lifetimes[50,51] is shown in Fig. 1. From these images (Fig. 7), intensity plots of delayed emission (Fig. 2) permit determination of a delay time for each image and further calculation of

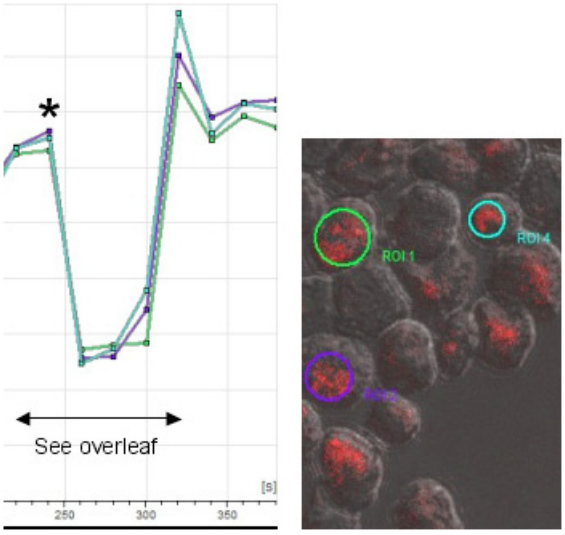

Fig. 6. Responses of Ru nanoparticles within MCF-7 cells in an anaerobic suspension (gas phase N_2) held in a hanging drop of growth medium to a one minute pulse of air. Time dependencies of intensities of emission from selected areas corresponding to three cells of the confocal image are indicated.

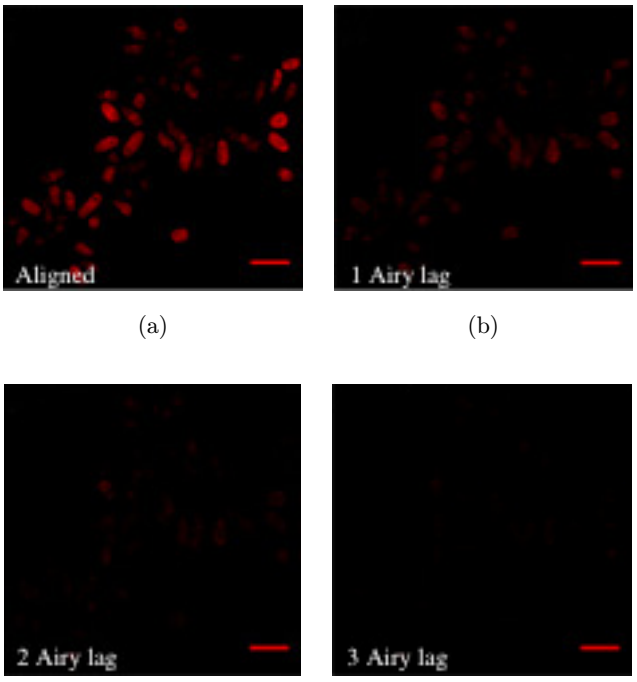

Fig. 7. Two-photon laser scanning confocal images of Ru nanoparticle-electroporated S. pombe acquired by using (a) the optically-aligned excitation beam, (b)–(d) the pinhole shift giving displacement by 1, 2 or 3 Airy units, respectively. Scale bars = 10 μm Reproduced with permission from Williams *et al.*[48]

phosphorescence lifetime. These images provide adequate resolution of the distribution of phosphorescence quenching within cells.

3.4. *Epi-phosphorescence microscopy*

The alternative strategy was to determine by single photon counting the phosphorescence emission of Ru nanoparticles from selected 0.5 μm diameter spots within cells. Following a single excitation pulse, a monophasic decay curve (Fig. 8) gave similar values for lifetimes to those obtained by the pinhole shifting method (Table 1).

Phosphorescence lifetimes give similar values by all three methods. For ethanol-fixed dead *Schizosaccharomyces pombe*, pinhole shifting under an anaerobic atmosphere gave a lifetime of 3.19 μs. This compared favorably with a corresponding value of 3.28 μs, using the epi-phosphorescence-TCSPC method, as well as a previously published value of 3.88 μs obtained using spectroscopy by Coogan *et al.*[32] (Table 1). Slight differences in lifetime values obtained from the latter method may be due to more efficient N_2 saturation of the cell or particle suspensions, whereby three cycles of O_2 evacuation were employed prior to generation of ananaerobic environment. Similar values were also obtained under air. For living organisms or cultured cells, shorter phosphorescence lifetimes indicated

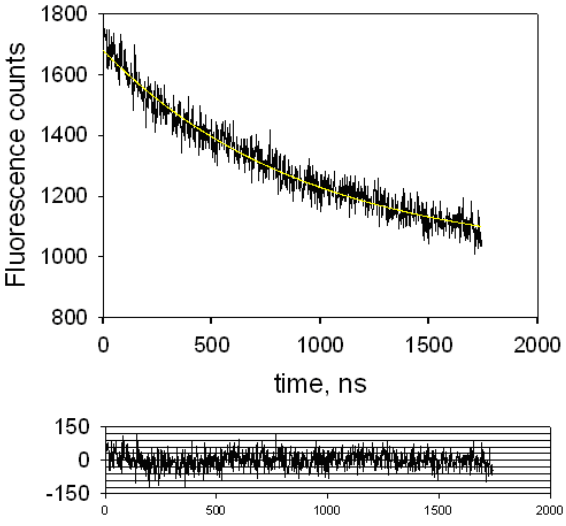

Fig. 8. Typical phosphorescence trace of Ru complex-loaded nanoparticles taken up by HDF cells. The value of the lifetime was 0.93 μs. The fitted line is shown as the smooth line. The bottom panel shows the residuals: these were due to the background counts recorded in complete darkness. Reproduced with permission from Williams *et al.*[48]

Table 1. Lifetime of Ru nanoparticles in suspension or electroporated into MCF-7, fixed yeast or HDF cells under different gas phases (expressed as equivalent dissolved $[O_2]$ mM), as assayed by spectrometry (Ru nanoparticles in suspension, or in MCF-7 cells (in parentheses)).[a]

Method employed	$[O_2]$ (mM)	Ru lifetime (μs)
Spectrometry[a] (Ru nanoparticles in suspension or in MCF-7 cells (in parenthesis))	0	3.88 (4.06)[b]
	0.26	1.81(2.29)
Pinhole shifting (fixed yeast)	0	3.19[b]
	0.01	2.86
	0	3.20
Epi-phosphorescence	0	3.28[c]
	0.26	0.95

Notes: [a]Coogan *et al.*[32]
Pinhole shifting (fixed yeast or HDF cells under aerobic (air) or anaerobic ([b]nitrogen or [c]argon), and epi-phosphorescence (TCSPC cells in buffer) methods.

quenching of Ru coordinate complex by intracellular O_2. Lifetime values obtained by epi-phosphorescence TCSPC differed amongst the varying biological specimens, for example MCF-7 cells showed lower O_2 concentrations than fibroblasts (Table 2), possibly due to the higher metabolic rates in the former.

These data also suggested slight differences between microsites within an individual cell, with higher O_2 concentrations near the periphery of the cytosol (Table 2). As yet, we have no values for intra-mitochondrial pO_2 where at the point of O_2 consumption values would be much lower.

Higher resolution of these subcellular structures would provide detailed maps of O_2 distribution in 3D using xy scans at successive z coordinates. For this, higher power objectives and appropriately adjusted parameters will be employed. Figure 9 shows atypical standard curve obtained from the

Table 2. Estimation of oxygen concentrations in MCF-7 and HDF cells by the epi-phosphorescence-TCSPC method.

		$[O_2]$ mM	
Cell type	Cell no.	Close to center	Close to plasma membrane
MCF-7	1	0.13	0.25
	2	0.12	0.18
	3	0.12	0.15
	4	0.13	0.20
	5	0.16	0.26
HDF	1	0.24	0.25
	2	0.21	0.27
	3	0.23	0.28
	4	0.19	0.27
	5	0.22	0.25

Notes: Each measurement corresponds to a different cell. Measurements made at regions either close to the center or close to the plasmamembrane were made in the same cell. Cells were equilibrated with air ($[O_2] = 0.26$ mM).

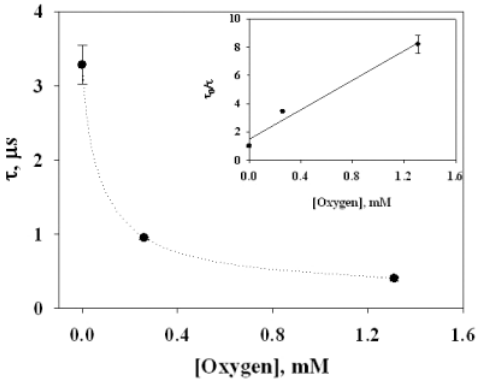

Fig. 9. Standard curve of phosphorescence lifetime vs concentration of oxygen in buffers saturated with nitrogen ($[O_2] = 0$), air ($[O_2] = 0.26$ mM) and oxygen ($[O_2] = 1.31$ mM) estimated by the epi-phosphorescence-TCSPC method. Standard deviations of 0.26, 0.02, and 0.02 were obtained respectively for the three values as estimated from eight independent measurements (shown as error bars). The inset shows the Stern–Volmer plot, namely $\tau_0/\tau = 1 + \tau_0 k_q [O_2]$, where τ_0 and τ are the phosphorescence lifetimes in the absence and the presence of quencher respectively and k_q is the bimolecular quenching constant. The estimated value of $k_q (= 1.46 \times 10^9\ M^{-1}\ s^{-1})$ is close to diffusion-controlled values as expected. Reproduced from Williams *et al.*,[48] with permission.

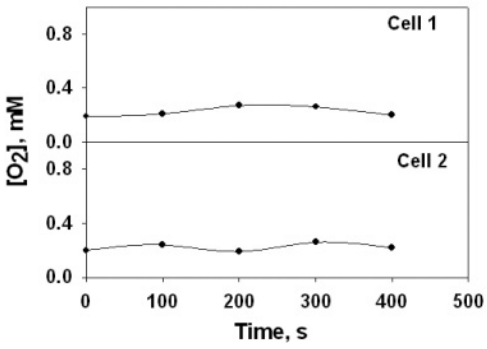

Fig. 10. Estimation of oxygen concentration in single HDF cells (equibrated in air) as a function of time. Phosphorescence from the entire cell was collected in these estimations made every 100 s. Time 0 refers to collection during 0–100 s and so on. Reproduced with permission from Williams *et al.*[48]

epi-phosphorescence-TCSPC method. This curve was used in estimations of O_2 concentrations inside a single HDF cell. Time-dependent variations in intracellular O_2 concentration, if confirmed in a more systematic study, would be useful in revealing metabolic oscillations.

Figure 9 shows a typical standard curve obtained from the epi-phosphorescence-TCSPC method. This curve was used in estimations of O_2 concentrations inside a single HDF cell (Table 2, Fig. 9). Time-dependent variations in intracellular O_2 concentration, if confirmed in a more systematic study, would be useful in revealing metabolic oscillations.

Major considerations of choice between the two methods employed in this study include the biological information required and cost. While raster scanning two-photon excitation potentially provides 3D rendered images, epi-phosphorescence photon quenching gives single point determinations. However, the cost implications of the former method are considerably greater.

Images obtained from two-photon excitation of a yeast (*S. pombe*) and a flagellate fish parasite (*Sp. vortens*) indicated the intracellular location and magnitude of O_2 gradients and confirmed the feasibility of optical mapping of cells and organisms under different external conditions. As well as obtaining measurements from single cells, Ru coordinate complex may prove useful to measure O_2 gradients in situ not only from intracellular sites, but also in interstitial extracellular locales (e.g., matrix elements in connective tissues) and in body fluids. However, further work is necessary to make reliable measurements of physiological significance.

Acknowledgments

David Lloyd wishes to express his indebtedness to Britton Chance for his enormous influence during David's pivotal and formative years and his continued interest and inspiration as a mentor and friend for 44 years. Of paramount importance were the daily meetings with visiting leaders in the field of bioenergetics, from the electric eel to avocado, *Vibrio fischeri* ("photobacterium") to *Arum spadix*, and from *Fasciola hepatica* to beef heart and mouse brain. Many major achievements were pioneered by the groups of workers at the Johnson Foundation at the University of Pennsylvania in the years while Britton Chance was its leader. These included the development of mechanical, electronic and optical devices that heralded a new era in the continuous non-invasive monitoring of living systems. As well as the establishment of a range of techniques for rapid reaction kinetics, the elucidation and definition of the respiratory states of mitochondria,[53] the first quantification of levels of tissue H_2O_2,[54] and the experimental demonstration of biological electron tunneling in membranes,[55] this laboratory was the first to exploit the diagnostic significance of intracellular redox states as monitored by NADH and flavin fluorescence, and its personell continue to exploit new clinical applications of this technique.[56]

Catrin F Williams held an EPSRC (EP/H501118/1) studentship with CASE Partner, Neem Biotech Ltd. G. Krishnamoorthy is a recipient of J. C. Bose National Research Fellowship of the Government of India. The authors thank Dr. Lars Folke Olsen, Dr. Allan Poulsen and Ms. Anita Lunding for expert guidance on nanoparticle preparation. Multiphoton confocal pinhole shifted laser scanning microscopy was carried out at the Vision Science Bioimaging Labs facility, School of Optometry and Vision Sciences, Cardiff University.

Note added after review. The high activity in this field is indicated by a plethora of new publications dated 2013, e.g., for brain and skin oxygenation in piglets,[57] in cortical arterioles,[58] in the rat retina,[59] and in mouse tumors.[60] A recent review of optical oxygen sensing concentrates on the quenching of phosphorescence.[61]

References

1. J. M. Vanderkooi, M. Erecinska I. A. Silver, "Oxygen in mammalian tissue: Methods of

measurement and affinities of various reactions," *Am. J. Physiol.* **260**, C1131–C1150 (1981).
2. B. A. Wittenberg, J. B. Wittenberg J. B. "Transport of oxygen in muscle," *Ann. Rev. Physiol.* **51**, 857–878 (1989).
3. D. B. Cater, S. Geraltini, F. Marina, I. Silver, "Changes in oxygen tension in brain and somatic tissues induced by vasodilator and vasoconstrictor substances," *Proc. R. Soc. B* **155**, 136–157 (1961).
4. M. Brezis S. Rosen P. Silva F. H. Epstein, "Renal ischemia in a new perspective," *Kidney Int.* **26**, 375–383 (1984).
5. G. Birol, S. Wang, E. Budzynski, N. D. Wangsa-Wirawan, R. A. Linsenmeier, "Oxygen distribution and consumption in the macaque retina," *Am. J. Physiol. Heart Circ. Physiol.* **293**, H1696–H1704 (2007).
6. G. He, R. A. Shankar, M. Chzhan, A. Samouilov, P. Kuppusamy, J. L. Zweier, "No-invasive measurement of anatomic structure and intraluminal oxygenation in the gastrointestinal tract of living mice with spatial and spectral imaging," *Proc. Nat. Acad. Sci. USA* **96**, 4586–4591 (1999).
7. D. Lloyd, S. Cortassa, B. O'Rourke, M. A. Aon, "What yeast and cardiomyocytes share: Ultradian oscillatory redox mechanisms of cellular coherence and survival," *Intgr. Biol.(Camb)* **4**, 65–74 (2012).
8. M. A. Aon, S. Cortassa, B. O'Rourke, "Redox-optimized ROS balance: A unifying hypothesis," *Biochem. Biophys. Acta* **1797**, 865–877 (2010).
9. C. Gitler, A. Danon, Eds., *Cellular Implications of Redox Signalling*, Imperial College Press, London (2003).
10. F. Schindler, Oxygen kinetics in the cytochrome oxygen reaction, Ph.D. Thesis, University of Pennsylvania, University Microfilms Inc., Ann Arbor, MI (1964).
11. B. Chance, S. Noka, W. Warren, G. Yurtsever, "Mitochondrial NADH as the bellwether of tissue O2 delivery," *Adv. Exp. Biol. Med.* **566**, 231–262 (2005).
12. D. P. Jones, H. S. Mason, "Gradients of O2 in hepatocytes," *J. Biol. Chem.* **253**, 4874–4880 (1978).
13. D. Lloyd, H. Mellor, J. L. Williams, "Oxygen affinity of the respiratory chain of *Acanthamoeba castellanii*", *Biochem. J.* **214**, 47–51 (1983).
14. G. L. Semenza, G. L. Wang, "A nuclear factor induced by hypoxia via de novo protein synthesis binds to the human erythropoietin gene enhancer at a site required for transcriptional acxtivation," *Mol. Cell. Biol.* **12**, 5447–5454 (1992).
15. C. T. Taylor, "Mitochondria and cellular oxygen sensing in the HIF pathway," *Biochem. J.* **409**, 19–26 (2008).
16. D. Lloyd, "Noninvasive methods for the investigation of organisms at low oxygen levels," *Adv. Appl. Microbiol.* **51**, 155–183 (2002).
17. D'Mello, S. Hill, R. K. Poole, "The oxygen affinity of cytochrome *bo*' in *Escherichia coli* determined by the deoxygenation of oxyleghaemoglobin and oxymyoglobin: Km values for oxygen are in the submicromolar range," *J. Bacteriol.* **177**, 867–870 (1995).
18. K. M. Lemar, M. A. Aon, S. Cortassa, B. O'Rourke, C. T. Muller, D. Lloyd "Diallyl disulphide depletes glutathione in *Candida albicans*: Oxidative-stress mediated cell death studied by 2-photon microscopy," *Yeast* **24**, 695–706 (2007).
19. M. P. Murphy, "How mitochondria produce reactive oxygen species," *Biochem. J.* **417**, 1–13 (2009).
20. S. A. Vinogradov, W. I. W. T. Jenkins, S. M. Evans, C. Koch, D. F. Wilson, "Non invasive imaging of the distribution oxygen in tissue in vivo using near infrared phosphors," *Biophys. J.* **70**, 1609–1617 (1996).
21. A. Devor, S. Sakadzic, S. A. Saisan, M. A. Yaseen, E. Roussakis, V. J. Srinivasan, S. A. Vinogradov, B. R. Buxton, A. M. Dale, D. A. Boas, "'Overshoot' of O_2 is required to maintain baseline tissue oxygenation at locations distal to blood vessels," *J. Neurosci.* **31**, 13676–13681 (2011).
22. K. Suhling, P. M. W. French, D. Phillips, "Time resolved fluorescence microscopy," *Photochem. Photobiol.* **4**, 13–22 (2004).
23. W. M. Vaughan, G. Weber, "Oxygen quenching of pyrene butyric acid fluorescence in water," *Biochemistry* **9**, 464–473 (1970).
24. D. H. Benson, J. A. Knopp, T. S. Longmuir, "Intracellular oxygen measurements of mouse liver cells using quantitative fluorescence microscopy," *Biochem. Biophys. Acta* **591**, 187–197 (1980).
25. G. T. Podgorski, I. S. Longmuir, J. A. Knopp, D. M. Benson, "Use of an encapsulated fluorescent probe to measure intracellular pO_2," *J. Cell Physiol.* **107**, 329–334 (1981).
26. M. Vanderkooi, G. Maniara, T. J. Green, D. F. Wilson, "An optical method for the measurement of dioxygen concentration based of phosphorescence," *J. Biol. Chem.* **262**, 3476–3482 (1987).
27. J. R. Bacon, J. N. Demas, "Determination of oxygen concentrations by luminescence quenching of a polymer immobilized transition-metal complex," *Anal. Chem.* **59**, 2780–2785 (1987).
28. D. Elson *et al.*, "Time-domain fluorescence lifetime imaging applied to biological tissue," *Photochem. Photobiol.* **3**, 795–801 (2004).
29. B. A. DeGraaf, J. N. Demas, "Luminescence-based oxygen sensors" *Reviews in Fluorescence*, C. Geddes and J. R. Lakowicz, Eds., Vol. 2, pp. 125–151, Springer, New York (2005).
30. A. J. Amoroso, M. P. Coogan, J. E. Dunne, V. Fernandez-Moreira, J. B. Hess, A. J. Hayes, D. Lloyd C. O. M. Millet, S. J. Pope, C. Williams, "Rhenium

fac-tricarbonyl bisimine complexes: Biologically useful flurochromes for cell imaging application," *Chem. Commun.* **29** 3066–3068 (2007).

31. A. J. Amoroso, R. J. Arthur, M. P. Coogan, J. B. Court, V. Fernandez-Moreira, A. J. Hayes, D. Lloyd C. Millet S. J. A. Pope, "3-Chloromethyl pyridyl bipyridine fac-tricarbonyl rhenium: A thiol-reactive luminophore for fluorescence microscopy accumulates in mitochondria," *New J. Chem.* **32**, 1097–1102 (2010).
32. M. P. Coogan, J. B. Court, V. L. Gray, A. J. Hayes, S. H. Lloyd, C. O. Millet, S. J. Pope, D. Lloyd "Probing intracellular oxygen by quenched phosphorescence lifetimes of nanoparticles containing polyacrylamide-embedded $[Ru(dpp(SO_3Na_2)_2]Cl_2$," *Photochem. Photobiol. Sci.* **9**, 103–109 (2010).
33. V. Fernandez-Moreira, F. L. Thorp-Greenwood, A. J. Amoroso, J. Cable, J. B. Court, V. Gray A. J. Hayes, R. J. Jenkins, B. M. Kariuki, D. Lloyd, C. O. Millet, C. F. Williams, M. P. Coogan, "Uptake and localisation of rhenium fac-tricarbonyl polypyridyls in fluorescent cell imaging-experiments," *Org. Biomol. Chem.* **8**, 3888–3901 (2010).
34. F. L. Thorp-Greenwood, V. Fernandez-Moreira, C. O. Millet, C. F. Williams, J. Cable, J. B. Court, A. J. Hayes, D. Lloyd, M. P. Coogan, "A 'Sleeping Trojan Horse' which transports metals into cells, localises in nucleoli, and has potential for biomodal fluorescence/PET imaging," *Chem. Commun.* **47**, 3096–3098 (2011).
35. R. G. Balasingham, F. L. Thorp-Greenwood, C. F. Williams, M. P. Coogan, S. J. Pope, "Biologically-compatible, phosphorescent dimetallic rhenium complexes linked through functionalized alkyl chains: Synthesis, spectroscopic properties, and applications in imaging microscopy," *Inorg. Chem.* **51**, 1419–1426 (2012).
36. R. J. Watts, G. A. Crosby, "Spectroscopic characterization of complexes of ruthenium (II) and iridium (II) with 4,4 diphenyl 2,2 bipyridine and 4,7-diphenyl-1,10-pehenanthroline," *J. Am. Chem. Soc.* **93**, 3184–3188 (1971).
37. F. N. Castellano, J. R. Lakowicz, "A water-soluble luminescence oxygen sensor," *Photochem. Photobiol.* **67**, 179–183 (1998).
38. A. Draaijer, A. Sanders, H. C. Yerritsen, "Fluorescence lifetime imaging, a new tool in confocal microscopy," *Handbook of Biological Confocal Microscopy*, 2nd Edition, J. B. Pawley Ed., pp. 491–505, Plenum, New York (1995).
39. A. Periasamy, P. Woodnicki, X. F. Wang, S. Kwon, G. W. Gordon, B. Herman, "A Time-resolved fluorescence lifetime imaging microscopy using a picosecond tuneable dye laser system," *Rev. Sci. Instrum.* **67**, 3722–3731 (1996).
40. K. J. Morris, M. S. Roach, W. Xu, J. N. Demas, B. A. DeGraff, "Luminescence lifetime standards for the nanosecond to microsecond range and oxygen quenching of Ru(II)," *Anal. Chem.* **79**, 9310–9314 (2007).
41. J. Zhong, M. Sakaki, H. Okada, E. T. Ahrens, "In vivo intracellular oxygen dynamics in murine brain glioma and immunotherapeutic response of cytotoxic T cells observed by Fluorine-19 magnetic resonance imaging," *Plos One* **8**(5) e59479 (2013).
42. S. W. Botchway, M. Charnley, J. W. Haycock, A. W. Parker, D. L. Rochester, J. A. Weinstein, J. A. Williams, "Time-resolved and two-photon emission imaging microscopy of live cells with inert platinum complexes," *Proc. Natl Acad. Sci. USA*, 105, 16071–16076 (2008).
43. H. A. Clark, M. Hoyer, M. A. Philbert, R. Kopelman, "Optochemical nanosensors for chemical analysis in living cells," *Anal. Chem.* **71**, 4831–4836 (1999).
44. S. M. Buck, Y. E. Koo, E. Park, H. Xu, M. A. Philbert, M. A. Basuel, R. Kopelman, "Optochemical nanosensor PEBBLEs: Photonic explorers for bioanalysis with biologically localized embedding," *Curr. Opin. Chem. Biol.* **8**, 540–546 (1999).
45. D. Lloyd, M. P. Coogan, S. J. A. Pope, "Novel metal-based luminophores for biological imaging," *Reviews in Fluorescence 2010*, C. D. Geddes, Ed., pp. 15–44, Springer, Business Media, New York (2012).
46. A. K. Poulsen, L. Arleth, K. Almdalk, A. M. Scharff-Poulsen, "Unusually large acrylamide induced effect on the droplet size in AOT/Brij30 water-in-oil emulsions," *J. Colloid Interface Sci.* **306**, 143–153 (2008).
47. A. K. Poulsen, A. M. Sharff-Poulsen, L. F. Olsen, "Horseradish peroxidase embedded in polyacrylamide nanoparticles enable optical detection of reactive oxygen species," *Anal. Biochem.* **366**, 29–36 (2007).
48. C. F. Williams, M. Kombrabail, K. Vijayalakshmi, N. White, G. Krishnamoorthy, D. Lloyd, "Technical Design Note: Evaluation of two novel methods for assessing intracellular O_2," *Meas. Sci. Technol.* **23**, 084005 (2012).
49. C. O. M. Millet, D. Lloyd, C. F. Williams, J. Cable "In vitro culture of the diplomonad fish parasite Spironucleus vortens reveals unusually fast doubling time and a typical biphasic growth," *J. Fish Dis.* **34**, 71–73 (2010).
50. V. K. Ramshesh, Luminescence lifetime imaging microscopy by confocal pinhole shifting (LLIM-CPS), Ph.D. Thesis, University of North Carolina at Chapel Hill, NC, USA (2007).
51. V. K. Ramshesh, J. J. Lemasters, "Pinhole shifting lifetime imaging microscopy," *J. Biomed. Opt.* **13**, 064001 (2008).

52. Y. D. Paila, M. Kombrabail, G. Krishnamoorthy, A. Chattopadhyay, "Oligomerization of the serotonin (1A) receptor in live cells: A time-resolved fluorescence anisotropy approach," *J. Phys. Chem. B* 115, 11439–11447 (2011).
53. B. Chance, G. R. Williams, "The respiratory chain and oxidative phosphorylation," *J. Biol. Chem.* **217**, 429–438 (1955).
54. D. DeVault, J. H. Parkes, B. Chance, "Electron tunnelling in cytochromes," *Nature*, **215**, 642–644 (1967).
55. B. Chance, H. Sies, A. Boveris, "Hydrogen peroxide metabolism in mammalian organs," *Physiol. Rev.* **59**, 527–605 (1979).
56. M. Matsubara, M. Ranji, B. G. Leshnower, M. Norma, S. J. Radcliff, B. Chance, R. C. Gorman, J. H. Gorman 3rd, "In vivo assessment of cyclosporine on mitochondrial function during myocardial ischemia and reperfusion," *Ann. Thorac. Surg.* **89**, 1532–1537 (2010).
57. D. F. Wilson, D. K. Harrison, "Simultaneous monitoring of brain and skin oxygenation during haemorrhagic shock in piglets," *Adv. Exp. Med. Biol.* **789**, 51–57 (2013).
58. S. M. Kasmi, A. J. Salvaggio, A. D. Estrada, M. A. Hemati, N. K. Shayduk, E. Roussakis, T. A. Jones, S. A. Vinogradov, A. K. Dunn, "Three-dimensional mapping of oxygen tension in cortical arterioles before and after occlusion," *Biomed. Opt. Express* **4**, 1061–1073 (2013).
59. J. Wanek, P. Y. Teng, N. P. Blair, M. Shahidi, "Inner retinal oxygen delivery and metabolism under normoxia and hypoxia in rat," *Invest. Opthalmol. Vis. Sci.* **54**, 5012–5019 (2013).
60. R. K. Jain, L. L. Munn, D. Fukumura, "Measuring interstitial pH and pO_2 in mouse tumors," *Cold Spring Harb. Protoc.* **7**, 678–680 (2013).
61. D. B. Papkovsky, R. I. Dmitriev, "Biological, detection by optical sensing," *Chem. Soc. Rev.* (June 2013), DOI: 10.1039/c3cs60131e.